ACS OMEGA

Open Access

http://pubs.acs.org/journal/acsodf

Article

Electrospun Manganese-Based Metal–Organic Frameworks for MnO_x Nanostructures Embedded in Carbon Nanofibers as a High-Performance Nonenzymatic Glucose Sensor

So Eun Kim, Jae Chol Yoon, Hyun-Jin Tae, and Alagan Muthurasu*

Cite This: *ACS Omega* 2023, 8, 42689–42698

Read Online

ACCESS | Metrics & More | Article Recommendations | Supporting Information

ABSTRACT: Material-specific electrocatalytic activity and electrode design are essential factors in evaluating the performance of electrochemical sensors. Herein, the technique described involves electrospinning manganese-based metal–organic frameworks (Mn-MOFs) to develop MnO_x nanostructures embedded in carbon nanofibers. The resulting structure features an electrocatalytic material for an enzyme-free glucose sensor. The elemental composition, morphology, and microstructure of the fabricated electrodes materials were characterized by using energy-dispersive X-ray spectroscopy (EDX), field-emission scanning electron microscopy (FESEM), and transmission electron microscopy (TEM). Cyclic voltammetry (CV) and amperometric $i-t$ (current–time) techniques are characteristically employed to assess the electrochemical performance of materials. The MOF MnO_x-CNFs nanostructures significantly improve detection performance for nonenzymatic amperometric glucose sensors, including a broad linear range (0 mM to 9.1 mM), high sensitivity (4080.6 μA mM^{-1} cm^{-2}), a low detection limit (0.3 μM, S/N = 3), acceptable selectivity, outstanding reproducibility, and stability. The strategy of metal and metal oxide-integrated CNF nanostructures based on MOFs opens interesting possibilities for the development of high-performance electrochemical sensors.

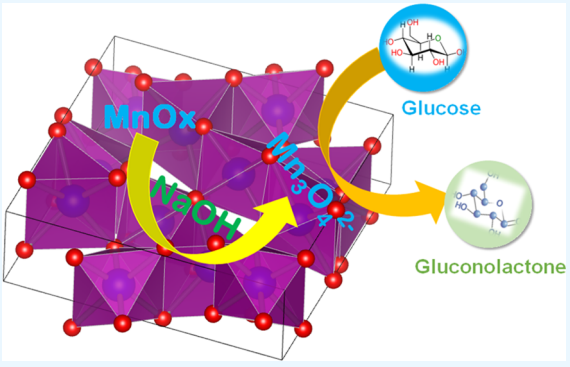

1. INTRODUCTION

Diabetes mellitus is a chronic metabolic disorder that occurs when the body is unable to properly process glucose (sugar) from food, and blood glucose levels rise above the normal range of 80–120 mg/dL (4.4–6.6 mM).[1,2] Chronically increased blood glucose levels can lead to a variety of health problems, including damage to the heart, blood vessels, nerves, kidneys, and eyes.[3] According to the International Diabetes Federation (IDF), more than 415 million people worldwide were diagnosed with diabetes in 2015.[4] Furthermore, the IDF predicts that if no major steps are taken to address this global health issue, diabetes will be the seventh leading cause of death by 2030.[5] In order to avoid the life-threatening diseases mentioned above, continuous monitoring of blood glucose levels is essential not only for diabetic patients but also for various other applications in the food industry and biotechnology.[6] It is critical to continually check glucose levels to monitor and control diabetes. However, collecting blood samples for analysis can be a painful and uncomfortable process for patients, and there is also the risk of cross-infection if the right safety measures are not accomplished.[7] Therefore, the significance of noninvasive, simple, and sensitive glucose examinations has been emphasized. Many noninvasive technologies are currently in development in a variety of industries.[8,9] Reverse iontophoresis,[10] absorbance spectroscopy,[11] and near-infrared spectroscopy[12] are a few examples. However, none of them have yet attained the sensitivity and precision required to completely replace finger-prick monitoring.[6,7] Minimally invasive glucose monitoring techniques can provide precise glucose monitoring while reducing the burden on a patient's quality of life.[13] These approaches have been frequently criticized for their difficulties, periodic calibration requirements, and sensitivity to biofouling, yet effective biosensor development can overcome these drawbacks.[6,13]

Over the years, several advanced glucose test detection technologies have been developed, including fluorescence spectroscopy,[14,15] chromatography,[16,17] colorimetry,[18−20] and electrochemical methods,[21−23] and they are all examples of analytical techniques. Electrochemical methods have gained significant attention in glucose determination due to their many advantages, including simplicity, rapidity, cost-effectiveness, high selectivity, and lower limit of detection.[24] It is important to note that enzyme-based glucose sensors have

Received: July 26, 2023
Revised: October 15, 2023
Accepted: October 17, 2023
Published: October 31, 2023

several limitations. Ongoing research and development efforts are focused on resolving these limitations and enhancing the overall performance and cost-effectiveness of these sensors.[25] Furthermore, there is a lack of stability under adverse environmental conditions such as temperature, pH, and humidity.[26,27] Enzyme-free glucose sensors are a promising alternative to traditional enzyme-based sensors. They rely on the direct electrocatalysis of glucose at the surface of the electrode rather than using an enzyme to catalyze the reaction.[28] This has several advantages such as cost-effectiveness, stability, and faster assay efficiency. The electrode material plays a crucial role in determining the electrocatalytic performance of a nonenzymatic sensor.[29] Electrode materials with enhanced conductivity and a large specific surface area can promote electron transfer occurring at the electrolyte/electrode interface, which is essential for the sensor's sensitivity and response time, and the electrode material should also have good biocompatibility.[30]

Transition metal oxides, such as manganese oxide (MnO_2),[31−33] cobalt oxide (Co_3O_4),[34−36] and nickel oxide (NiO),[37−39] have shown promise as electrocatalysts in various electrochemical applications, including sensing and biosensing. Among them, MnO_2 exhibits unique electronic and electrochemical properties that make it an attractive material for glucose sensor fabrication.[40] The material has a high surface area and good conductivity, which enables it to efficiently catalyze the oxidation of glucose molecules.[41] Additionally, the intrinsic redox behavior of MnO_2 (Mn^{3+}/Mn^{4+}) allows for the material to act as an electron mediator, facilitating the transfer of electrons between the glucose molecules and the electrode surface.[42] Due to its physical and electrochemical characteristics, MnO_2 is widely acknowledged as the perfect substance for biosensor applications.[43] MnO_2 exists in multiple forms, including α-, β-, γ-, λ-, and δ-type, which are determined by the different connections of MnO_6 octahedron units. The research on glucose sensing using MnO_2 has predominantly centered around the α-type due to its distinctive 2×2 and 1×1 tunnels that facilitate electrode kinetics.[44] Despite these advantages, there are relatively few MnO_2-based glucose sensors reported in the literature.[33] Xiao et al. developed a procedure involving electrodeposition to promote an interconnected PtAu alloy and MnO_2 on self-supporting graphene paper, creating a nonenzymatic glucose sensor.[42] Weina et al. conducted a study using β-MnO_2 on carbon fibers as an electrode material to investigate its importance in the electrochemical sensing of glucose.[31] They also tested β-MnO_2 for dopamine sensing and analyzed the probabilities of dopamine binding using docking analysis.[45] Additionally, the MnO_2/GO composite, known for its strong catalytic activity, has been utilized as a heterogeneous catalyst in the aerobic oxidation of benzyl alcohol.[46] Among the various MnO_x nanostructures investigated, a metal−organic framework (MOF)-based MnO_x nanostructure has gained increasing attention in recent years due to its unique design and advantages in various applications.[47] The active element (for example, MnO_x) is enclosed within a hollow shell in the yolk−shell structure, leaving a void in the center. Additionally, the void space in the center can be used for various purposes, such as accommodating more active material to boost electrochemical activity.[48] Despite the excellent electrocatalytic activity, the low electronic conductivity of metal oxides can limit the efficiency of electrocatalysis and its application in electrochemistry. The most common approach to overcome this limitation is to build hybrid electrodes that combine nanostructured metal oxides and highly conductive materials.[49] In this scenario, an electrospun carbon nanofiber (CNF) is considered a potentially promising candidate to make hybrid nanostructures by an electrospinning method.[31] Particularly, the well-aligned CNF structure can act as a scaffold to support the metal oxide nanostructures, and the alignment of the CNF structure is important because it can reduce the distance electrons must travel through the material, improving conductivity and lead to a composite material with improved properties for electrochemical sensing applications.[32]

According to the aforementioned aspects, herein, we propose a simple method for synthesizing nonenzymatic glucose sensor electrocatalysts employing a manganese-based metal−organic framework (Mn-BTC) electrospun into carbonized fibers (MOF MnO_x-CNFs). The electrode architecture has robust electrical conductivity, which enables efficient electron transport to target molecules, such as glucose, increasing sensing efficiency. For glucose detection, the MOF MnO_x-CNFs-modified electrode demonstrates remarkable sensitivity, quick response time, outstanding selectivity, and a wide linear detection range. These features are due to the improved electroactive sites, excellent conductivity, extremely high catalytic activity of MOF MnO_x-CNFs, and stability of the three-dimensional framework. The combination of the MOF MnO_x with CNFs exhibits a synergistic effect, resulting in a hybrid material with improved glucose oxidation activity. This hybrid material is anticipated to outperform the individual MOF MnO_x, CNF, and bare GCE systems. Furthermore, MOF MnOx-CNFs have shown potential reliability for glucose detection in human serum.

2. EXPERIMENTAL SECTION

2.1. Chemicals. $Mn(NO_3)_2{\cdot}4H_2O$ (98+%, Sigma-Aldrich), C_2H_5OH (Sigma-Aldrich), trimesic acid (1,3,5-H_3BTC) (98%, Sigma-Aldrich), *N*,*N*-dimethylformamide (DMF) (≥99.5%), and polyacrylonitrile (PAN) (Mw 200,000, Sigma-Aldrich) were used as obtained. Sodium hydroxide (NaOH), potassium ferricyanide ($K_3Fe(CN)_6$), glucose ($C_6H_{12}O_6$), dopamine (DA), L-ascorbic acid (AA), and uric acid (UA) were obtained from Sigma-Aldrich. All compounds were of analytical reagent quality and were utilized without additional purification.

2.2. Synthesis of MOF Mn Spheres. In brief, 0.188 g of $Mn(NO_3)_2{\cdot}4H_2O$ was added to 50 mL of ethanol and dissolved completely to make solution A. After that, 30 mL of ethanol was used to dissolve 0.088 g of 1,3,5-H_3BTC to make solution B. Then, solution B was mixed with solution A to form a uniform solution. After stirring for 20 min, the mixture was transferred to a 100 mL Teflon-lined stainless-steel autoclave. The mixture was then heated to 160 °C for 12 h. Finally, the obtained powder was washed five times with ethanol and dried at 60 °C for 12 h in an electric oven to obtain the MOF Mn spheres.

2.3. Fabrication of MOF MnO_x-CNFs. First, 0.5 g of PAN was added to 5 g of DMF to form a homogeneous solution. The solution was then stirred at 50 °C to obtain a pale-yellow clear solution. Second, after cooling to room temperature, 0.25 g of MOF Mn spheres was dispersed in the above solution. The mixture solution was transferred to a 5 mL plastic syringe fitted with a plastic nozzle. The needle and collector, which were separated by 15 cm, were then supplied with a high output potential of 17 kV. The feeding rate, temperature, and relative humidity (RH) were all set to 1 mL/h, 25 °C, and 45 ± 3, respectively. The obtained film was then dried at 60 °C

https://doi.org/10.1021/acsomega.3c05459
ACS Omega 2023, 8, 42689−42698

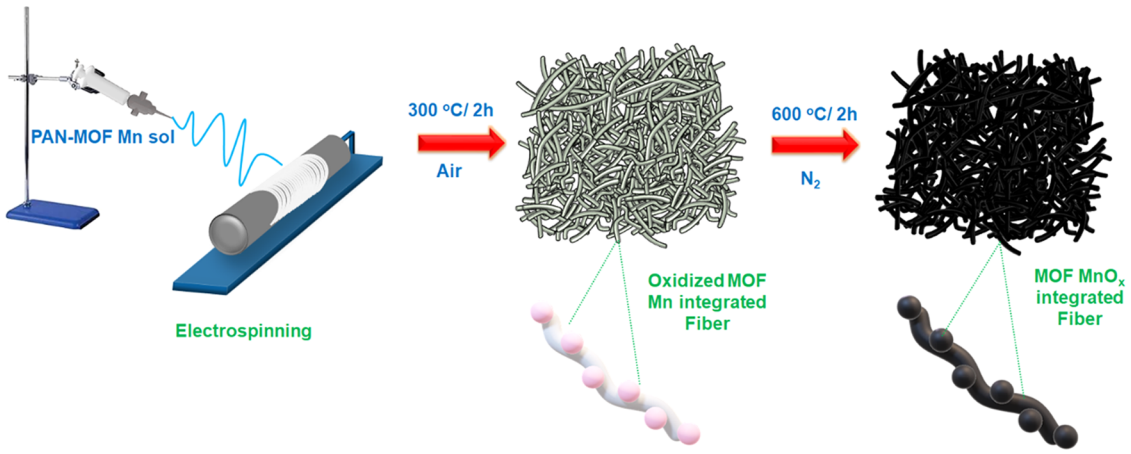

Figure 1. Schematic representation of the fabrication method for MOF MnO_x-CNFs.

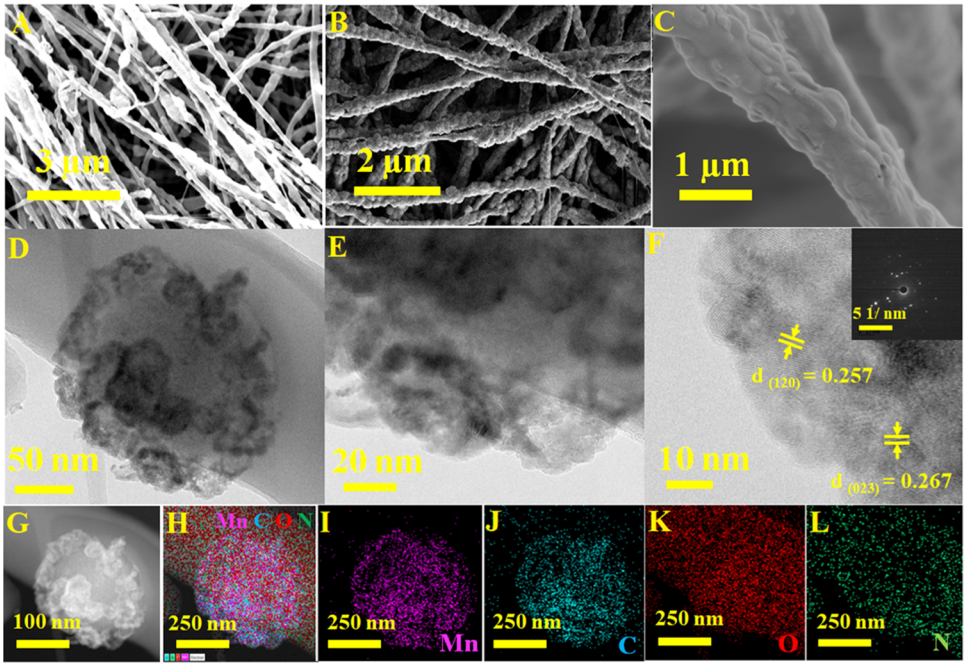

Figure 2. Different magnifications of (A, B, C) FESEM images, (D, E) TEM images, (F) high-magnification TEM (inset is the corresponding SAED image), and (G–L) TEM-EDX mapping of Mn, C, O, and N of MOF MnO_x-CNFs.

overnight, and the electrospun PAN mat was stabilized at 300 °C with a ramping rate of 2 °C min^{-1} for 2 h. Subsequently, carbonization of the preoxidized fiber mat was continued by heating the film at a ramping rate of 2.5 °C min^{-1} up to 600 °C and keeping it for 2 h in a tubular furnace under an N_2 environment. The obtained films were named MOF MnO_x-CNFs. MOF Mn spheres were also calcined under the same conditions without the use of electrospinning.

2.4. Material Characterizations. The surface morphology of materials was determined by a Hitachi S-7400 (Japan). The Hitachi S-7400, FESEM model is designed to produce high-quality images at a variety of magnifications. The crystal structure and defects within the material were examined using a high-resolution transmission electron microscope (JEOL Ltd., Japan JEM-2100 200 kV). The JEOL Ltd. (Japan) JEM-2100 200 kV is a specific model of HRTEM that can provide high-quality images of nanofibers. The elemental composition of a sample is detected and measured using an energy-dispersive X-ray spectrometer. X-ray photoelectron spectroscopy (XPS) is a technique for determining the chemical composition of a material. A Thermo Scientific KA 1066 instrument with a monochromatic Al Kα X-ray source was employed for this analysis. The crystal structure was identified by X-ray diffraction (Rigaku Co., Japan). The Raman spectra of carbonized nanofibers were obtained by using an RFS-100S evolution spectrometer from Bruker (Germany).

2.5. Preparation of the MOF MnO_x-CNFs-Modified Electrode. Prior to modification, the GCE was polished with 0.05 mm alumina and thoroughly rinsed with DI water and acetone. After that, 5 min of ultrasonic cleaning in DI water and air drying were carried out. 5 mg of MOF MnO_x-CNFs material was dispersed in 1 mL of ethanol–water (v/v = 1:3) and 10 μL of 5% Nafion solution, which was then constantly sonicated to generate a uniform ink mixture. Afterward, 10 μL of MOF MnO_x-CNFs material ink dispersion was drop cast onto the cleaned GCE surface and dried in a hot air oven. And the prepared electrode is called MOF MnO_x-CNFs/GCE. When not in use, the modified electrodes were kept at room

https://doi.org/10.1021/acsomega.3c05459
ACS Omega 2023, 8, 42689–42698

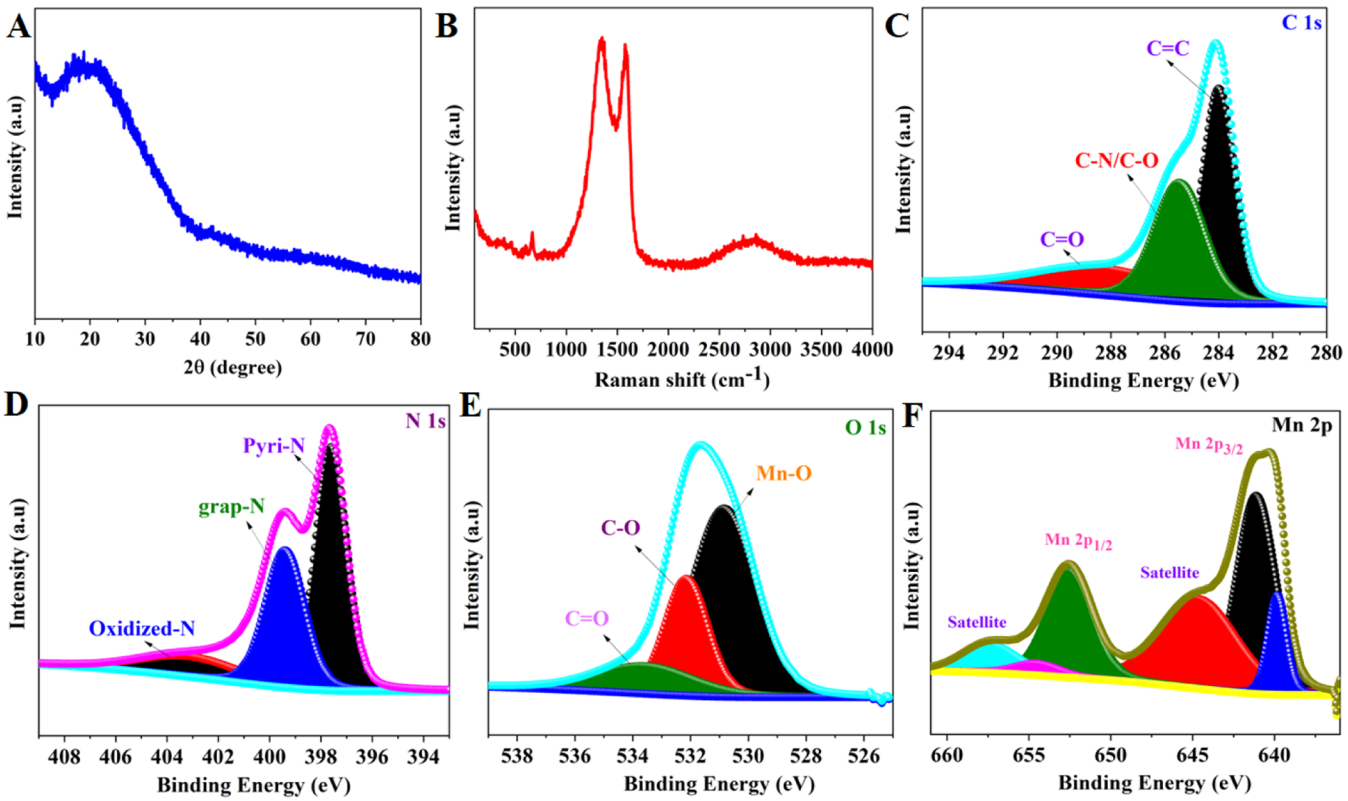

Figure 3. (A) XRD patterns, (B) Raman spectra, and high-resolution XPS spectra of MOF MnO_x-CNFs: (C) C 1s, (D) N 1s, (E) O 1s, and (F) Mn 2p.

temperature. Cyclic voltammetry (CV), chronoamperometry (CA), and electrochemical impedance spectroscopy (EIS) experiments were performed using VersaSTAT 4 electrochemical analyzers and a typical three-electrode electrochemical workstation. The three-electrode electrochemical system comprised of a MOF MnO_x-CNFs/GCE electrode as the working electrode and a platinum wire and saturated KCl and Ag/AgCl as the counter electrode and reference electrode, respectively, and all tests were conducted at room temperature. Typically, the electrolyte solution is the 0.1 M NaOH solution used in glucose sensors. We also employed our newly developed sensor to evaluate glucose levels in human serum samples (Jeonbuk University Institute of Medicine).

3. RESULTS AND DISCUSSION

The fabrication route of MOF MnO_x-CNFs is schematically shown in Figure 1. The Experimental Section describes the experiment in detail. Briefly, the MOF Mn spheres are a crystalline structure prepared via a hydrothermal reaction in an aqueous solution containing Mn(II)-based compounds and trimesic acid. The MOF Mn spheres have an average size of roughly 300 nm and are uniform in structure (Figure S1). After that, an electrospun solution of PAN and MOF Mn spheres in *N*,*N*-dimethylformamide (DMF) was used to produce a fibrous membrane. The synthesis membrane consists of randomly aligned microfibers that are linked together to form a network. Each hybrid fiber comprises MOF Mn spheres that are evenly distributed throughout the fiber. As illustrated in Figure S2, the hybrid fiber's surface structure is porous and rough. After that, the resultant fiber membrane is then preoxidized in air at 300 °C for 2 h and carbonized in N_2 gas at 600 °C. The fiber shape is highly retained after heat treatment, and the MOF MnO_x is uniformly dispersed in the carbon fiber. The FESEM images in Figure 2 demonstrate that the MOF MnO_x-CNFs have nitrogen-doped carbon. FESEM elemental mapping and EDX spectra are shown in Figure S3. The MOF MnO_x-CNFs show average diameters of 350 nm. The magnified FESEM image (Figure 2B,C) and transmission electron microscopy (TEM) image (Figure 2D) demonstrate that the microfibers are composed of MOF MnO_x-CNFs that are linked together by a carbon matrix generated from PAN. MOF MnO_x particles are dispersed with mild aggregation in both cavities and within a portion of the solid PAN-derived carbon fibers. These findings are depicted in magnified TEM images in Figure 2E. MOF MnO_x is found inside the yolk and appears darker than the surrounding carbon matrix. High-magnification TEM images of MnO_x nanoparticles on the shell of MOF MnO_x-CNFs (Figure 2F) show 0.257 and 0.267 nm lattice fringe planes compatible with the (120) and (023) planes of orthorhombic Mn_3O_4, respectively (JCPDS No. 65-1123).[50] The inset of Figure 2F shows the polycrystalline character of the shell in the selected area electron diffraction pattern (SAED). MOF MnO_x-CNFs were analyzed by bright-field STEM and subsequent EDX elemental mapping (Figure 2G−L). The findings of the study revealed a homogeneous distribution of four elements within the membrane: manganese (Mn), carbon (C), nitrogen (N), and oxygen (O). The existence of Mn, C, N, and O in the MOF MnO_x-CNFs is also revealed by the EDX spectrum (Figure S4).

The X-ray diffraction pattern in Figure 3A reveals broad peaks with no significant diffraction peaks, demonstrating the presence of carbon layer enclosing the MnO_x nanoparticles in the MOF MnO_x-CNFs composites. The X-ray diffraction (XRD) patterns of a MnO_x sample are illustrated in Figure S5.

https://doi.org/10.1021/acsomega.3c05459
ACS Omega 2023, 8, 42689−42698

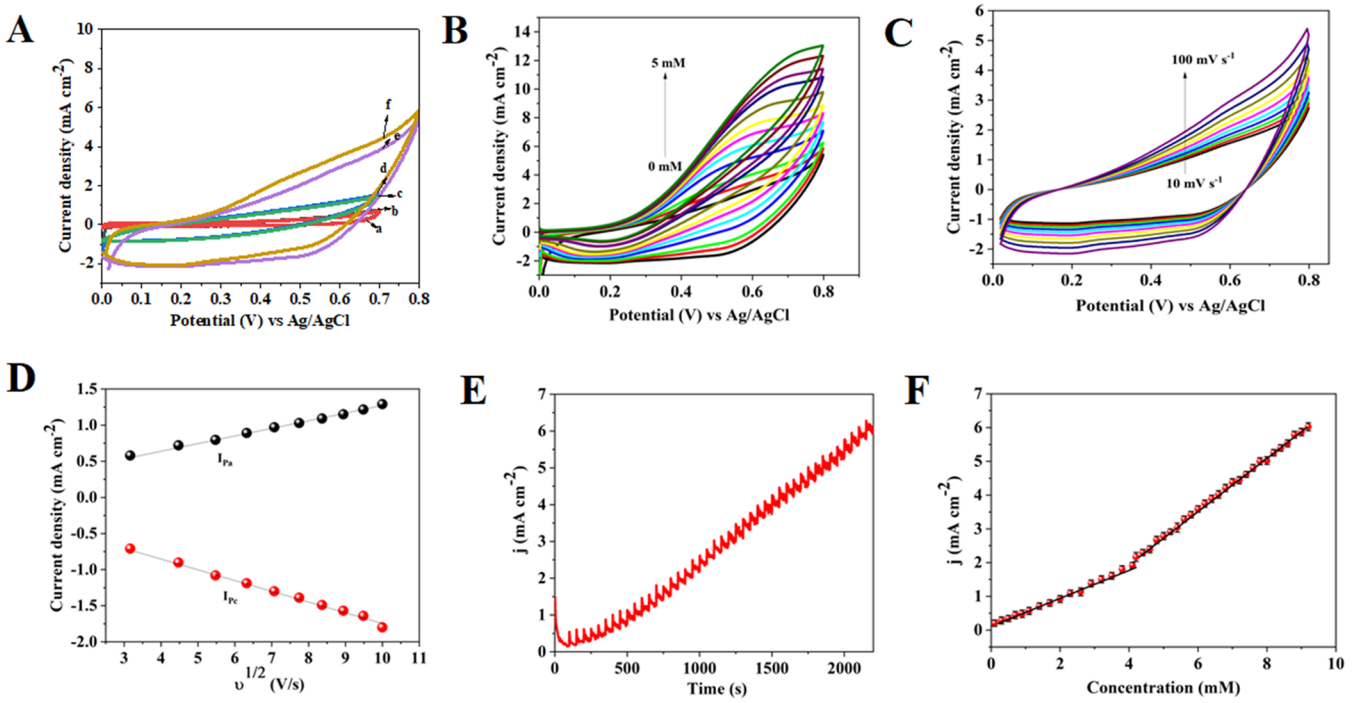

Figure 4. (A) CV curves of the (a, b) bare GCE, (c, d) MOF MnO_x, and (e, f) MOF MnO_x-CNFs-modified GCE without and with the presence of glucose recorded at a scan rate of 50 mV s^{-1}, (B) CV curves of MOF MnO_x-CNFs-modified GCE recorded at the scan rate of 50 mV s^{-1} in the presence of various glucose concentrations, (C) CV curves of MOF MnO_x-CNFs-modified GCE electrode at different scan rates from 10 to 100 mV s^{-1} in 0.1 M NaOH with 0.1 mM glucose, (D) corresponding calibration plot of peak current (I_p) vs square root of scan rate ($\sqrt{\nu}$), (E) amperometric response of the MOF MnO_x-CNFs-modified GCE electrode under successive addition of various concentrations of glucose, and (F) calibration curve of current density vs concentration of glucose.

The peaks observed at 34.8, 40.5, 58.6, and 70.1° correspond to the crystal planes (111), (200), (220), and (311) of the cubic phase of MnO (JCPDS = 78-0424). Raman spectroscopy is an effective tool to investigate material molecular vibrations and structural characteristics. The Raman spectra of carbonized PAN fibers display two notable peaks known as the D and G bands. The D band appears at approximately 1354 cm^{-1}, whereas the G band appears at around 1590 cm^{-1}. These bands are typical of graphitic carbon structures. Additionally, the incorporation of Mn-BTC resulted in an intensity of 676 cm^{-1} at the Mn−O stretching frequency, and the broad peak in the 2500−3000 cm^{-1} range is associated with the C−H stretching vibrations in organic molecules (CNF), showing that the carbonized fibers were successfully packed with MnO_x species (Figure 3B). X-ray photoelectron spectroscopy (XPS) is a technique for determining the elemental composition and chemical states of a material's surface. XPS survey spectra from the MOF MnO_x-CNFs composite revealed the presence of C, N, O and Mn (Figure S6). The high-resolution C 1s spectrum of the MOF MnO_x-CNFs composite was deconvoluted into three peaks. Each peak corresponds to a different carbon species. The binding energies associated with these subpeaks are 284.1, 285.6, and 288.6 eV, corresponding to the carbon species C═C, C−N/C−O, and C═O (Figure 3C).[26] The high-resolution N 1s spectrum (Figure 3D) contains three deconvoluted peaks with different binding energies: 397.7, 399.4, and 403.2 eV.[51] Each peak represents a different nitrogen species, such as pyridinic, graphitic, and oxidized nitrogen. Figure 3E exhibits a high-resolution O 1s spectrum with a strong peak found at 530.8 eV. This peak indicates the presence of a Mn−O bond, confirming the presence of MnO_x.[32] The binding energy peaks of Mn $2p_{1/2}$ and $2p_{3/2}$ in the high-resolution Mn 2p spectra are 652.6 and 641.2 eV, respectively (Figure 3F). These findings suggest that the oxidation state of manganese (Mn) in the samples fluctuates between Mn^{2+} (MnO) and Mn^{3+} (Mn_2O_3).[33,50]

The prepared MOF MnO_x-CNFs electrode was scanned by using cyclic voltammetry (CV) in a 0.1 M NaOH electrolyte at a scan rate of 50 mV s^{-1} until the CV curves entirely overlapped. This technique is likely to activate and stabilize the electrochemical performance of the electrode. Following that, CV was used to study the electrochemical properties of a MOF MnO_x-CNFs electrode in a 0.1 M NaOH electrolyte with and without the addition of glucose, and the electrode was scanned within a potential window of 0.0 and 0.8 V vs Ag/AgCl. Figure 4A demonstrates the CV curves of three separate samples, MOF MnO_x-CNFs, MOF MnO_x, and bare GCE materials are recorded in the presence of 0 and 0.1 mM glucose. There is no redox peak in the CV curve of the bare CC. This implies that at the investigated potential range, the bare GCE exhibits no electrochemical activity. Furthermore, the CV curve of the bare GCE does not alter significantly when glucose is added. This suggests that the presence of glucose has no noticeable impact on the electrochemical behavior of the bare GCE. On the other hand, in the absence of glucose, the MOF MnO_x-CNFs/GCE electrode exhibits a broad shoulder oxidation peak extending from 0.15 to 0.55 V. This implies that a redox reaction is taking place in this potential range, most likely related to the oxidation or reduction of Mn_3O_4/MnOOH and MnOOH/MnO_2 species.[31,33] When glucose (0.1 mM glucose) is introduced, the anodic (oxidation) peak current of the MOF MnO_x-CNFs/GCE electrode considerably increases. This suggests that the electrode has outstanding catalytic ability for glucose oxidation. In comparison to MOF MnO_x-CNFs/

https://doi.org/10.1021/acsomega.3c05459
ACS Omega 2023, 8, 42689−42698

GCE, the current response of MOF MnO_x after glucose addition is significantly lower. Previous research suggests that the catalytic glucose oxidation pathway might involve the following[33,48,49]

$$MnO_2 + 2OH^- \rightarrow MnO_4^{2-} \quad (1)$$

$$MnO_4^{2-} + \text{glucose} \rightarrow \text{gluconolactone} + MnO_2 + 2OH^- \quad (2)$$

$$\text{gluconolactone} \rightarrow \text{gluconicacid} \quad (3)$$

The CV curve of the MOF MnO_x-CNFs/GCE in the glucose concentration range of 0−5.0 mM is shown in Figure 4B. The data reveal that the peak anodic current of the MOF MnO_x-CNFs/GCE increases as the glucose concentration increases. All of these results indicate that the MOF MnO_x-CNFs/GCE exhibits potential glucose oxidation activity. To investigate the effect of the scan rates, CV curves for the MOF MnO_x-CNFs/GCE was obtained at various scan rates ranging from 10 to 100 mV s^{-1} (Figure 4C). The square root of the scan rate and peak current had a nearly parallel linear relationship. The oxidation reaction appears to be a diffusion-controlled process based on the linear relationship between the square root of the scan rate and peak current (Figure 4D). The two linear regression equations are formulated as follows: $E_{pa} = 0.2478 + 0.075g\nu$ ($R^2 = 0.992$) and $E_{pc} = 0.1292 - 0.060 \lg \nu$ ($R^2 = 0.991$), which match the black and red dotted lines (Figure 5c). According to Laviron's

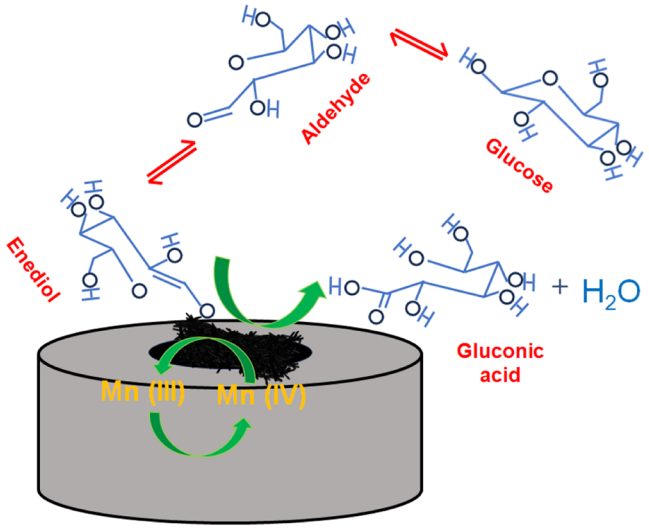

Figure 5. Mechanism of the electro-oxidation of glucose at the MOF MnO_x-CNFs@GCE electrode.

equation, the transfer coefficient (α) and the number of electrons transported (n) were computed. Their values were 1.512 and 0.469, showing that electron-transfer kinetics during electrocatalytic processes are relatively fast.[23,47]

$$E_{pa} = E^0 + 2.3(RT/(1-\alpha)nF) \lg \nu \quad (4)$$

$$E_{pc} = E^0 - 2.3(RT/\alpha nF) \lg \nu \quad (5)$$

where n is the number of electrons transferred, α is the electron-transfer coefficient, ν is the scan rate, and E^0 is the formal potential. F, R, and T have traditional connotations.

The applied potential can have an effect on the response current and enhance the sensor performance of the modified electrode. Figure S7 shows how the amperometry response curves of glucose obtained at the MOF MnO_x-CNFs/GCE electrode with successive injections of 1.0 mM glucose changed as the applied potential varied from 0.4 to 0.55 V. The response current increases as the potential increases from 0.4 to 0.55 V, suggesting a positive relationship between the applied potential and the response current. However, above 0.55 V, the response current drops as the applied potential increases, indicating a negative correlation. Therefore, the response current of the system is maximum at 0.55 V, indicating the most efficient glucose detection and measurement. The detection performance of a MOF MnO_x-CNFs/GCE electrode for glucose detection may be affected by the concentrations of OH^- anions (C_{OH^-}) in the alkali electrolyte. This is because the electrochemical activity is closely related to the C_{OH^-} levels under alkaline conditions.[52] To achieve maximum glucose oxidation current, we examined the impact of C_{OH^-} on the amperometric reaction toward glucose oxidation in the MOF MnO_x-CNFs/GCE, using NaOH solution with varying concentrations and an applied potential near the anodic peak. In a continuous stirred solution of NaOH, glucose was added at incremental concentrations. Regardless of the different NaOH concentrations, the amperometry curves all demonstrated a rapid increase in current upon the addition of glucose, as depicted in Figure S8. The performance of the MOF MnO_x-CNFs/GCE for glucose detection in a 0.1 M NaOH solution showed significant improvements in sensitivity, detection limit, and linear range compared to the performance in 0.1, 0.25, 0.5, 0.75, and 1 M NaOH solutions. In our investigations, we determined that an OH^- anion concentration of 0.1 M is the most suitable working electrolyte for glucose detection.

Amperometry is a technique that measures the current response of an electrode as a function of the analyte concentration. Each addition of glucose is performed at 60 s intervals with an applied potential of 0.55 V. Figure 4E clearly depicts a series of stepwise $i-t$ curves in response to continuous glucose additions. This indicates that the oxidation current appears to increase with each addition of glucose, implying a possible relationship between the observed current and the concentration of glucose. It is worth noting that upon the addition of glucose, a response signal is immediately observed and stabilizes within 3 s. This indicates that the detection performance is quick and sensitive. The reason for this performance is considered to be the good electrocatalytic properties mentioned above. As illustrated in Figure 4F, a calibration curve is developed to measure the concentration of glucose by detecting changes in current density. The calibration curve shows that the current density increases linearly with an increase in glucose concentration. The glucose oxidation of MOF MnO_x-CNFs/GCE can be categorized into two ranges of linear functions for concentrations of 0 to 4.1 mM and 4.1 to 9.1 mM with R^2 of 0.998. Furthermore, based on the slope of the calibration curve, the sensitivity of 0−4.1 mM is calculated to be 4080.6 μA mM^{-1} cm^{-2}. The limit of detection (LOD) is a measurement of the lowest concentration of an analyte estimated to be 0.3 μM by using the calibration curve's sensitivity and a signal-to-noise ratio (SNR) of 3. The calibration curves show two different linear curves that could be caused by distinct reasons. The first linear fit implies that the electro-oxidation of the glucose reaction is

https://doi.org/10.1021/acsomega.3c05459
ACS Omega 2023, 8, 42689−42698

Table 1. Comparison of the Analytical Performance of Manganese Oxide-Based Glucose Sensors

electrode	optimal potential (V)	linear range	sensitivity/μA cm^{-2} mM^{-1}	detection limit (μM)	refs
MnO_2/Co_3O_4@ECNFs	0.55	5 μM−1.93 mM	1159	0.3	48
GOx/MnO_2/MWCNTs/GCE	0.55	5−200 μM		2	33
α-MnO_2	0.45	5−855 μM	3730		32
MnO_2/MWNT	0.55	0−1 mM	3406	0.5	49
Cu/MnO_2/MWCNTs	0.6	0.64−2200 μM	1302	1.7	54
$CoFe_2O_4$ @MnO_2	0.25	0.53−1300 μM	318	0.325	55
Ni/MnO_2	0.45	0.25−3500 μM	104.0	0.1	56
Cu/MnO_2/GCE	0.7	0.25−1.02 μM	26.96	0.1	57
PVA/MnO_2@GO/CuO MIP		0.55−4.4 mM		53	58
MnO_2/Co_3O_4	0.55	0−7 mM	127	0.3	59
MnO_2/gra-H	0.45	0−5.0 mM	45	0.08	41
Pd/MnO_2	0.45	65−455 μM	6.0		40
MnO_2 NS/NF	0.45	0.001−1.13 mM	6.45	0.5	60
MOF MnO_x-CNFs	**0.55**	**0−9.10**	**4080.6**	**0.3**	**this work**

limited by glucose absorption onto electrochemically active sites, which is followed by redox reaction and charge transfer. In the second linear range of 4.1−9.1 mM, MOF MnO_x-CNFs provide an optimal environment to allow efficient adsorption of glucose molecules and desorption of reaction byproducts.[53] In particular, the sensing characteristics of the MOF MnO_x-CNFs/GCE electrode are among the best-reported values for nonenzymatic sensors based on nanostructured materials (Table 1).[54−60] The outstanding catalytic activity of MOF MnO_x-CNFs in glucose oxidation can be attributed to the following factors. First, the combination of manganese oxide nanoparticles with carbon nanofibers in MOF MnO_x-CNFs has a synergistic effect. MOF MnO_x particles serve as active catalytic sites, while CNFs provide structural stability and electron conductivity.[42] This synergy increases the effective electron transfer throughout the oxidation reaction, resulting in improved catalytic performance. Second, manganese oxide is well-known for its outstanding oxidation and reduction properties.[50] It is capable of redox reactions during the glucose oxidation process, enhancing electron transport and increasing the conversion of glucose to a desirable product.

The mechanism for detecting glucose using the MOF MnO_x-CNFs electrode is explained in Figure 5. Mn(III) undergoes electro-oxidation to Mn(IV), a highly reactive compound that reacts with glucose adsorbed on the surface of MOF MnO_x-CNFs. This reaction oxidizes glucose into gluconic acid, after which Mn(IV) is reduced to Mn(III). As this cycle repeats, the generated electrons from the electro-oxidation of Mn(III) travel through the nanostructure to the conductive substrate below, resulting in the detection of an anodic signal.[46,47,57]

The stability, repeatability, and selectivity of biosensors are critical parameters in their practical application. Monitoring the sensitivity of the MOF MnO_x-CNFs electrode to 0.1 mM glucose was performed on a regular basis to determine its stability over time. Figure S9A shows that after 30 days, the fabricated sensor retains approximately 94.2% of its initial amperometric current response. This indicates that the sensor exhibits a relatively stable performance over a period of time, with a slight decrease in the amperometric current response. In terms of reproducibility, 10 MOF MnO_x-CNFs electrodes were made under identical conditions and then individually tested for their current responses to a glucose concentration of 0.1 mM, as shown in Figure S9B. These findings show that the MOF MnO_x-CNFs electrode has excellent stability and reproducibility. In addition, the selectivity of the MOF MnO_x-CNFs electrode refers to its ability to detect and quantify a specific analyte in the presence of simultaneous interferences in human blood, such as dopamine (DA), ascorbic acid (AA), uric acid (UA), and chloride ions. As shown in Figure 6, the interference of specific species in the presence of glucose in human blood is 30 times greater than that of the interfering species. To begin, 1 mM glucose was added to a 0.1 M NaOH solution. Then, 0.1 mM interfering species was added to the same solution. When a 1 mM glucose solution was injected, the oxidation current increased immediately. However, subsequent injections of DA, AA, and UA had no significant effect on the current response when compared to the glucose injection. Even though these three specific interferents can oxidize at low potentials, the ensuing signals are feeble. These findings indicate that these interferences have a minor effect on the electrocatalysis current response at the conditions investigated. This means that the MOF MnO_x-CNFs electrode has good selectivity for detecting glucose because the presence of these interfering chemicals does not affect them.

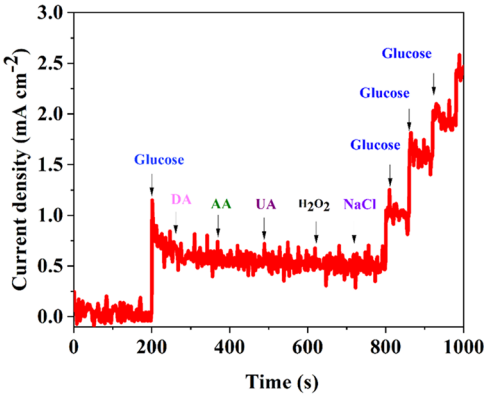

Figure 6. Amperometry responses of MOF MnO_x-CNFs-modified GCE recorded in 1.0 mM glucose and under the sequential influence of electroactive interferences, namely, 0.5 mM AA, 0.1 mM DA, 0.1 mM UA, and 0.5 mM KCl.

It is vital to emphasize the practical necessity of using sensors in serum samples. The MOF MnO_x-CNFs electrode is used as an electrode material for amperometric glucose concentration determination in human serum samples.

https://doi.org/10.1021/acsomega.3c05459
ACS Omega 2023, 8, 42689−42698

Human serum samples of different concentrations were added to a stirred solution of 0.1 M NaOH, and the amperometric response was measured by using an electrode at an applied voltage of 0.55 V. Table 2 shows that the addition of serum causes a noticeable change in the electrical current. The electrical current increases in proportion to the serum concentration, showing a relationship between the two parameters. MOF MnO_x-CNFs/GCE electrode test findings with commercial blood glucose devices indicate that the MOF MnO_x-CNFs/GCE electrode is a potential tool for detecting glucose levels in real samples. This study shows that the composite electrode could be employed in practical applications, such as glucose monitoring for medical purposes or the development of glucose sensing devices.

Table 2. Glucose Detection in Human Serum Samples

sample	added (mM)	found (mM)	RSD% (n = 3)	recovery (%)
1	1.25	1.29	3.5	103.2
2	2.01	1.95	3.0	97.0
3	3.28	3.35	3.6	103.3
4	5.80	5.65	4.5	95.9
5	8.49	8.32	2.67	97.9

4. CONCLUSIONS

In summary, using MOF Mn spheres as the structural template, our study successfully used electrospinning to generate MnO_x nanoparticles confined in nitrogen-doped carbon fibers. Incorporating MOF MnO_x structures into carbonized nanofibers improved nanostructures. Benefits include improved structural integrity, increased electrical conductivity, and an increased electrochemically active surface area. The MOF MnO_x-CNFs electrode used as an active material in an enzymeless glucose sensor has been found to have improved sensitivity and a low detection limit. The MOF MnO_x-CNFs composite has an excellent electrocatalytic oxidation performance for glucose. This improved performance can be attributed to two key factors: the compact structure and the synergistic effect of MOF MnO_x and CNFs. Moreover, the MOF MnO_x-CNFs electrode addressed above is well-known for fulfilling the selectivity, stability, and reproducibility criteria. Our method for fabricating MOF metal oxide with CNFs offers new avenues for developing nanohybrid electrodes with tailored compositions and functionality. This nanohybrid electrode could be a potential candidate for nonenzymatic glucose sensors.

■ ASSOCIATED CONTENT

Supporting Information

The Supporting Information is available free of charge at https://pubs.acs.org/doi/10.1021/acsomega.3c05459.

Detailed material characterization, including SEM images, elemental mapping, EDX spectra, XRD patterns, XPS survey spectra, CA curves, and current response of different time intervals and various electrodes (PDF)

■ AUTHOR INFORMATION

Corresponding Author

Alagan Muthurasu − *Department of Nano Convergence Technology, Jeonbuk National University, Jeonju 54907, Republic of Korea;* orcid.org/0000-0002-2137-1703; Email: amuthurasu@gmail.com

Authors

So Eun Kim − *Department of Emergency Medicine, Research Institute of Clinical Medicine of Jeonbuk National University and Biomedical Research Institute of Jeonbuk National University Hospital, Jeonju 54907, Republic of Korea*

Jae Chol Yoon − *Department of Emergency Medicine, Research Institute of Clinical Medicine of Jeonbuk National University and Biomedical Research Institute of Jeonbuk National University Hospital, Jeonju 54907, Republic of Korea*

Hyun-Jin Tae − *College of Veterinary Medicine and Biosafety Research Institute, Jeonbuk National University, Iksan 54596, Republic of Korea*

Complete contact information is available at: https://pubs.acs.org/10.1021/acsomega.3c05459

Notes

The authors declare no competing financial interest.

■ ACKNOWLEDGMENTS

This study was supported by the Fund of the Biomedical Research Institute and Jeonbuk National University Hospital and by the Research Funds for Newly Appointed Professors of Jeonbuk National University in 2023.

■ REFERENCES

(1) Witkowska Nery, E.; Kundys, M.; Jeleń, P. S.; Jönsson-Niedziólka, M. Electrochemical Glucose Sensing: Is There Still Room for Improvement? *Anal. Chem.* **2016**, *88* (23), 11271−11282.

(2) Teymourian, H.; Barfidokht, A.; Wang, J. Electrochemical Glucose Sensors in Diabetes Management: An Updated Review (2010−2020). *Chem. Soc. Rev.* **2020**, *49* (21), 7671−7709.

(3) Feng, Y.; Xiang, D.; Qiu, Y.; Li, L.; Li, Y.; Wu, K.; Zhu, L. MOF-Derived Spinel NiCo2O4 Hollow Nanocages for the Construction of Non-Enzymatic Electrochemical Glucose Sensor. *Electroanalysis* **2020**, *32* (3), 571−580.

(4) Naikoo, G. A.; Salim, H.; Hassan, I. U.; Awan, T.; Arshad, F.; Pedram, M. Z.; Ahmed, W.; Qurashi, A. Recent Advances in Non-Enzymatic Glucose Sensors Based on Metal and Metal Oxide Nanostructures for Diabetes Management- A Review. *Front. Chem.* **2021**, *9* (September), No. 748957.

(5) Cho, N. H.; Shaw, J. E.; Karuranga, S.; Huang, Y.; da Rocha Fernandes, J. D.; Ohlrogge, A. W.; Malanda, B. IDF Diabetes Atlas: Global Estimates of Diabetes Prevalence for 2017 and Projections for 2045. *Diabetes Res. Clin. Pract.* **2018**, *138*, 271−281.

(6) Ahmed, I.; Jiang, N.; Shao, X.; Elsherif, M.; Alam, F.; Salih, A.; Butt, H.; Yetisen, A. K. Recent Advances in Optical Sensors for Continuous Glucose Monitoring. *Sens. Diagn.* **2022**, *1* (6), 1098−1125.

(7) Sun, M. T.; Li, I. C.; Lin, W. S.; Lin, G. M. Pros and Cons of Continuous Glucose Monitoring in the Intensive Care Unit. *World J. Clin. Cases* **2021**, *9* (29), 8666−8670.

(8) Ma, R.; Shao, R.; An, X.; Zhang, Q.; Sun, S. Recent Advancements in Noninvasive Glucose Monitoring and Closed-Loop Management Systems for Diabetes. *J. Mater. Chem. B* **2022**, *10* (29), 5537−5555.

(9) Pors, A.; Rasmussen, K. G.; Inglev, R.; Jendrike, N.; Philipps, A.; Ranjan, A. G.; Vestergaard, V.; Henriksen, J. E.; Nørgaard, K.; Freckmann, G.; Hepp, K. D.; Gerstenberg, M. C.; Weber, A. Accurate Post-Calibration Predictions for Noninvasive Glucose Measurements in People Using Confocal Raman Spectroscopy. *ACS Sens.* **2023**, *8*, 1272−1279.

(10) Zhu, W.; Yu, H.; Pu, Z.; Guo, Z.; Zheng, H.; Li, C.; Zhang, X.; Li, J.; Li, D. Effect of Interstitial Fluid PH on Transdermal Glucose Extraction by Reverse Iontophoresis. *Biosens. Bioelectron.* **2023**, *235* (May), No. 115406.
(11) Nguyen, S. H.; Vu, P. K. T.; Nguyen, H. M.; Tran, M. T. Optical Glucose Sensors Based on Chitosan-Capped ZnS-Doped Mn Nanomaterials. *Sensors* **2023**, *23* (5), 2841.
(12) Srichan, C.; Srichan, W.; Danvirutai, P.; Ritsongmuang, C.; Sharma, A.; Anutrakulchai, S. Non-Invasively Accuracy Enhanced Blood Glucose Sensor Using Shallow Dense Neural Networks with NIR Monitoring and Medical Features. *Sci. Rep.* **2022**, *12* (1), No. 1769.
(13) Lee, H.; Hong, Y. J.; Baik, S.; Hyeon, T.; Kim, D. H. Enzyme-Based Glucose Sensor: From Invasive to Wearable Device. *Adv. Healthcare Mater.* **2018**, *7* (8), No. 1701150.
(14) Zhang, L.; Zhang, Z. Y.; Liang, R. P.; Li, Y. H.; Qiu, J. D. Boron-Doped Graphene Quantum Dots for Selective Glucose Sensing Based on the "Abnormal" Aggregation-Induced Photoluminescence Enhancement. *Anal. Chem.* **2014**, *86* (9), 4423−4430.
(15) Shen, P.; Xia, Y. Synthesis-Modification Integration: One-Step Fabrication of Boronic Acid Functionalized Carbon Dots for Fluorescent Blood Sugar Sensing. *Anal. Chem.* **2014**, *86* (11), 5323−5329.
(16) Xie, W. Q.; Gong, Y. X.; Yu, K. X. Rapid Quantitative Detection of Glucose Content in Glucose Injection by Reaction Headspace Gas Chromatography. *J. Chromatogr. A* **2017**, *1520*, 143−146.
(17) Zhou, Y. Y.; Chen, J. P.; Gan, L.; Xu, W.; Liu, Y.; Zhao, Y. G.; Zhu, Y. A Non-Invasive Method for the Detection of Glucose in Human Exhaled Breath by Condensation Collection Coupled with Ion Chromatography. *J. Chromatogr. A* **2022**, *1685*, No. 463564.
(18) Kangkamano, T.; Witsapan, W.; Numnuam, A.; Subba, J. R.; Jayeoye, T. J. Colorimetric Hydrogen Peroxide and Glucose Sensors Based on the Destruction of Micelle-Protected Iron(Ii) Complex Probes. *New J. Chem.* **2023**, *47*, 11261−11274.
(19) Ding, W.; Liu, H.; Zhao, W.; Wang, J.; Zhang, L.; Yao, Y.; Yao, C.; Song, C. A Hybrid of FeS2Nanoparticles Encapsulated by Two-Dimensional Carbon Sheets as Excellent Nanozymes for Colorimetric Glucose Detection. *ACS Appl. Bio Mater.* **2020**, *3* (9), 5905−5912.
(20) Kap, Ö.; Kılıç, V.; Hardy, J. G.; Horzum, N. Smartphone-Based Colorimetric Detection Systems for Glucose Monitoring in the Diagnosis and Management of Diabetes. *Analyst* **2021**, *146* (9), 2784−2806.
(21) Muthurasu, A.; Ganesh, V. Glucose Oxidase Stabilized Fluorescent Gold Nanoparticles as an Ideal Sensor Matrix for Dual Mode Sensing of Glucose. *RSC Adv.* **2016**, *6* (9), 7212−7223.
(22) Radhakrishnan, S.; Lakshmy, S.; Santhosh, S.; Kalarikkal, N.; Chakraborty, B.; Rout, C. S. Recent Developments and Future Perspective on Electrochemical Glucose Sensors Based on 2D Materials. *Biosensors* **2022**, *12* (7), 467.
(23) Hwang, D. W.; Lee, S.; Seo, M.; Chung, T. D. Recent Advances in Electrochemical Non-Enzymatic Glucose Sensors − A Review. *Anal. Chim. Acta* **2018**, *1033*, 1−34.
(24) Chen, C.; Xie, Q.; Yang, D.; Xiao, H.; Fu, Y.; Tan, Y.; Yao, S. Recent Advances in Electrochemical Glucose Biosensors: A Review. *RSC Adv.* **2013**, *3* (14), 4473−4491.
(25) Lipińska, W.; Siuzdak, K.; Karczewski, J.; Dołęga, A.; Grochowska, K. Electrochemical Glucose Sensor Based on the Glucose Oxidase Entrapped in Chitosan Immobilized onto Laser-Processed Au-Ti Electrode. *Sens. Actuators, B* **2021**, *330*, No. 129409.
(26) Muthurasu, A.; Kim, H. Y. Fabrication of Hierarchically Structured MOF-Co 3 O 4 on Well-Aligned CuO Nanowire with an Enhanced Electrocatalytic Property. *Electroanalysis* **2019**, *31* (5), 966−974.
(27) Yang, J.; Lin, Q.; Yin, W.; Jiang, T.; Zhao, D.; Jiang, L. A Novel Nonenzymatic Glucose Sensor Based on Functionalized PDDA-Graphene/CuO Nanocomposites. *Sens. Actuators, B* **2017**, *253*, 1087−1095.
(28) Su, Y.; Guo, H.; Wang, Z.; Long, Y.; Li, W.; Tu, Y. Au@Cu2O Core-Shell Structure for High Sensitive Non-Enzymatic Glucose Sensor. *Sens. Actuators, B* **2018**, *255*, 2510−2519.
(29) Wei, M.; Qiao, Y.; Zhao, H.; Liang, J.; Li, T.; Luo, Y.; Lu, S.; Shi, X.; Lu, W.; Sun, X. Electrochemical Non-Enzymatic Glucose Sensors: Recent Progress and Perspectives. *Chem. Commun.* **2020**, *56* (93), 14553−14569.
(30) Daud, A. D.; Lim, H. N.; Ibrahim, I.; Endot, N. A.; Gowthaman, N. S. K.; Jiang, Z. T.; Cordova, K. E. An Effective Metal-Organic Framework-Based Electrochemical Non-Enzymatic Glucose Sensor. *J. Electroanal. Chem.* **2022**, *921* (May), No. 116676.
(31) Weina, X.; Guanlin, L.; Chuanshen, W.; Hu, C.; Wang, X. A Novel β-MnO2Micro/Nanorod Arrays Directly Grown on Flexible Carbon Fiber Fabric for High-Performance Enzymeless Glucose Sensing. *Electrochim. Acta* **2017**, *225*, 121−128.
(32) Ponnusamy, R.; Venkatesan, R.; Kandasamy, M.; Chakraborty, B.; Rout, C. S. MnO2 Polymorph Selection for Non-Enzymatic Glucose Detection: An Integrated Experimental and Density Functional Theory Investigation. *Appl. Surf. Sci.* **2019**, *487* (May), 1033−1042.
(33) Hao, L.; Li, S. S.; Wang, J.; Tan, Y.; Bai, L.; Liu, A. MnO2/Multi-Walled Carbon Nanotubes Based Nanocomposite with Enhanced Electrocatalytic Activity for Sensitive Amperometric Glucose Biosensing. *J. Electroanal. Chem.* **2020**, *878*, No. 114602.
(34) Kannan, P.; Maiyalagan, T.; Marsili, E.; Ghosh, S.; Guo, L.; Huang, Y.; Rather, J. A.; Thiruppathi, D.; Niedziolka-Jönsson, J.; Jönsson-Niedziolka, M. Highly Active 3-Dimensional Cobalt Oxide Nanostructures on the Flexible Carbon Substrates for Enzymeless Glucose Sensing. *Analyst* **2017**, *142* (22), 4299−4307.
(35) Xu, H.; Xia, C.; Wang, S.; Han, F.; Akbari, M. K.; Hai, Z.; Zhuiykov, S. Electrochemical Non-Enzymatic Glucose Sensor Based on Hierarchical 3D Co3O4/Ni Heterostructure Electrode for Pushing Sensitivity Boundary to a New Limit. *Sens. Actuators, B* **2018**, *267*, 93−103.
(36) Liaqat, I.; Iqbal, N.; Aslam, M.; Nasir, M.; Hayat, A.; Han, D. X.; Niu, L.; Nawaz, M. H. Co3O4 Nanocubes Decorated Single-Walled Carbon Nanotubes for Efficient Electrochemical Non-Enzymatic Glucose Sensing. *SN Appl. Sci.* **2020**, *2* (10), 1−12.
(37) Bach, L. G.; Thi, M. L. N.; Bui, Q. B.; Nhac-Vu, H. T. Hierarchical Cobalt Nanorods Shelled with Nickel Oxide Vertically Attached 3D Architecture as Non-Binder and Free-Standing Sensor for Sensitive Non-Enzymatic Glucose Detection. *Mater. Res. Bull.* **2019**, *118* (April), No. 110504.
(38) Kim, S. E.; Muthurasu, A. Metal-Organic Framework−Assisted Bimetallic Ni@Cu Microsphere for Enzyme-Free Electrochemical Sensing of Glucose. *J. Electroanal. Chem.* **2020**, *873*, No. 114356.
(39) Prasad, R.; Bhat, B. R. Multi-Wall Carbon Nanotube-NiO Nanoparticle Composite as Enzyme-Free Electrochemical Glucose Sensor. *Sens. Actuators, B* **2015**, *220*, 81−90.
(40) Ponnusamy, R.; Gangan, A.; Chakraborty, B.; Late, D. J.; Rout, C. S. Improved Nonenzymatic Glucose Sensing Properties of Pd/MnO2 Nanosheets: Synthesis by Facile Microwave-Assisted Route and Theoretical Insight from Quantum Simulations. *J. Phys. Chem. B* **2018**, *122* (31), 7636−7646.
(41) Chang, H. W.; Dong, C. L.; Chen, Y. H.; Xu, Y. Z.; Huang, T. C.; Chen, S. C.; Liu, F. J.; Lai, Y. H.; Tsai, Y. C. Extended Graphite Supported Flower-like Mno2 as Bifunctional Materials for Supercapacitors and Glucose Sensing. *Nanomaterials* **2021**, *11* (11), 2881.
(42) Xiao, F.; Li, Y.; Gao, H.; Ge, S.; Duan, H. Growth of Coral-like PtAu-MnO2 Binary Nanocomposites on Free-Standing Graphene Paper for Flexible Nonenzymatic Glucose Sensors. *Biosens. Bioelectron.* **2013**, *41* (1), 417−423.
(43) Huang, J.; Zeng, Q.; Wang, L. Ultrasensitive Electrochemical Determination of Ponceau 4R with a Novel ϵ-MnO2Microspheres/Chitosan Modified Glassy Carbon Electrode. *Electrochim. Acta* **2016**, *206*, 176−183.
(44) Han, L.; Shao, C.; Liang, B.; Liu, A. Genetically Engineered Phage-Templated MnO2 Nanowires: Synthesis and Their Application

https://doi.org/10.1021/acsomega.3c05459
ACS Omega 2023, 8, 42689−42698

in Electrochemical Glucose Biosensor Operated at Neutral PH Condition. *ACS Appl. Mater. Interfaces* **2016**, *8* (22), 13768−13776.
(45) Divagar, M.; Sriramprabha, R.; Ponpandian, N.; Viswanathan, C. Highly Selective and Sensitive Electrochemical Detection of Dopamine with Hydrothermally Prepared β-MnO2 Nanostructures. *Mater. Sci. Semicond. Process.* **2018**, *83*, 216−223.
(46) Kadam, M. M.; Dhopte, K. B.; Jha, N.; Gaikar, V. G.; Nemade, P. R. Synthesis, Characterization and Application of γ-MnO2/Graphene Oxide for the Selective Aerobic Oxidation of Benzyl Alcohols to Corresponding Carbonyl Compounds. *New J. Chem.* **2016**, *40* (2), 1436−1442.
(47) Zhang, Y.; Huang, Y.; Gao, P.; Yin, W.; Yin, M.; Pu, H.; Sun, Q.; Liang, X.; Fa, H. bao. Bimetal-Organic Frameworks MnCo-MOF-74 Derived Co/MnO@HC for the Construction of a Novel Enzyme-Free Glucose Sensor. *Microchem. J.* **2022**, *175*, No. 107097.
(48) Ma, X.; Tang, K. Lai.; Yang, M.; Shi, W.; Zhao, W. Metal−Organic Framework-Derived Yolk−Shell Hollow Ni/NiO@C Microspheres for Bifunctional Non-Enzymatic Glucose and Hydrogen Peroxide Biosensors. *J. Mater. Sci.* **2021**, *56* (1), 442−456.
(49) Guo, C.; Li, H.; Zhang, X.; Huo, H.; Xu, C. 3D Porous CNT/MnO2 Composite Electrode for High-Performance Enzymeless Glucose Detection and Supercapacitor Application. *Sens. Actuators, B* **2015**, *206*, 407−414.
(50) Li, Y.; Tang, L.; Deng, D.; He, H.; Yan, X.; Wang, J.; Luo, L. Hetero-Structured MnO-Mn3O4@rGO Composites: Synthesis and Nonenzymatic Detection of H2O2. *Mater. Sci. Eng., C* **2021**, *118*, No. 111443.
(51) Kim, S. E.; Muthurasu, A. Highly Oriented Nitrogen-Doped Carbon Nanotube Integrated Bimetallic Cobalt Copper Organic Framework for Non-Enzymatic Electrochemical Glucose and Hydrogen Peroxide Sensor. *Electroanalysis* **2021**, *33*, 1333−1345.
(52) Li, H.; Zhang, L.; Mao, Y.; Wen, C.; Zhao, P. A Simple Electrochemical Route to Access Amorphous Co-Ni Hydroxide for Non-Enzymatic Glucose Sensing. *Nanoscale Res. Lett.* **2019**, *14*, No. 135.
(53) Yin, Z.; Allado, K.; Sheardy, A. T.; Ji, Z.; Arvapalli, D.; Liu, M.; He, P.; Zeng, X.; Wei, J. Mingled MnO2and Co3O4Binary Nanostructures on Well-Aligned Electrospun Carbon Nanofibers for Nonenzymatic Glucose Oxidation and Sensing. *Cryst. Growth Des.* **2021**, *21* (3), 1527−1539.
(54) Wang, Y.; Zhang, S.; Bai, W.; Zheng, J. Layer-by-Layer Assembly of Copper Nanoparticles and Manganese Dioxide-Multiwalled Carbon Nanotubes Film: A New Nonenzymatic Electrochemical Sensor for Glucose. *Talanta* **2016**, *149*, 211−216.
(55) He, G.; Wen, Y.; Ma, C.; Wang, L.; Gao, L.; Sun, Z. Detection of Glucose Using a Thin-Walled Honeycombed MnO2 Grown on Mesoporous CoFe2O4 Nanosheets. *Colloids Surf., A* **2023**, *660*, No. 130817.
(56) Wang, Y.; Bai, W.; Nie, F.; Zheng, J. A Non-Enzymatic Glucose Sensor Based on Ni/MnO2 Nanocomposite Modified Glassy Carbon Electrode. *Electroanalysis* **2015**, *27* (10), 2399−2405.
(57) Meng, Z.; Sheng, Q.; Zheng, J. A Sensitive Non-Enzymatic Glucose Sensor in Alkaline Media Based on Cu/MnO2-Modified Glassy Carbon Electrode. *J. Iran. Chem. Soc.* **2012**, *9* (6), 1007−1014.
(58) Farid, M. M.; Goudini, L.; Piri, F.; Zamani, A.; Saadati, F. Molecular Imprinting Method for Fabricating Novel Glucose Sensor: Polyvinyl Acetate Electrode Reinforced by MnO2/CuO Loaded on Graphene Oxide Nanoparticles. *Food Chem.* **2016**, *194*, 61−67.
(59) Sinha, L.; Pakhira, S.; Bhojane, P.; Mali, S.; Hong, C. K.; Shirage, P. M. Hybridization of Co3O4 and α-MnO2 Nanostructures for High-Performance Nonenzymatic Glucose Sensing. *ACS Sustainable Chem. Eng.* **2018**, *6* (10), 13248−13261.
(60) Huang, M.; Feng, S.; Yang, C.; Wen, F.; He, D.; Jiang, P. Construction of an MnO2nanosheet Array 3D Integrated Electrode for Sensitive Enzyme-Free Glucose Sensing. *Anal. Methods* **2021**, *13* (10), 1247−1254.

https://doi.org/10.1021/acsomega.3c05459
ACS Omega 2023, 8, 42689−42698